A comparative analysis of frequency- and impulse-based substructuring for experimental shock response predictions

F. Trainotti, O. M. Zobel, D. J. Rixen
Technical University of Munich, Chair of Applied Mechanics, TUM School of Engineering and Design,
Boltzmannstr. 15, 85748 Garching, Germany
e-mail: **francesco.trainotti@tum.de**

Abstract
Frequency-based substructuring has become widely adopted in experimental settings due to its ease of use, and counts numerous successful applications. In the analysis of shock and initial response peaks, however, a frequency domain prediction might be erroneous due to the artifacts of the Fourier transform, such as the forced periodization. The issue might be addressed via impulse-based substructuring, the time domain counterpart of the frequency-based formulation, which utilises impulse response functions and linear convolution for the coupling process. This article presents a comparative analysis of frequency- and impulse-based substructuring techniques in the context of experimental shock response predictions. First, time and frequency domain deconvolution algorithms are discussed and compared on a numerical example. Then, the outcome of a substructuring prediction is demonstrated in an experimental coupling scenario. Both a one-dimensional rod and a multi-dimensional virtual point coupling applications are presented.

1 Introduction

Dynamic Substructuring is an engineering concept where a large, complex assembly is divided into subcomponents, the equations of motion are solved at the local level, and then the subcomponents are reassembled through interface conditions. Due to its simplicity and robustness, a frequency-based coupling formulation, i.e. Frequency-Based Substructuring (FBS) [1, 2], has become established in both academic and industrial practice. Several engineering applications require the correct estimation of the response to a shock (e.g. a falling smartphone), where one is interested in the initial maximum stresses/amplitudes rather than the long-term oscillation of the system. For these applications, time-based processing seems more natural. Further, it would avoid any frequency transformation that could introduce artifacts into the desired time response prediction. Hence the concept of Impulse-Based Substructuring (IBS), originally coined in [3, 4] and later formulated in the dual assembly framework in [5]. The experimental application of IBS with its advantages and limitations has recently been demonstrated in [6]. Despite their theoretical equivalence for linear time-invariant systems, IBS and FBS are founded on different data processing algorithms, which may lead to divergent outcomes.
This paper presents a comparative study between frequency-based and impulse-based substructuring for the prediction of shock responses in experimental scenarios. This includes the analysis and theoretical understanding of deconvolution approaches that are inherently part of the measurement-assembly-prediction data processing chain. Emphasis is placed on the influence of random errors in the inverse estimation. The proposed time and frequency substructuring workflows are then compared on two experimental benchmarks of increasing complexity. The effectiveness and limitations of both strategies are discussed with examples.
The theoretical basis for the application of deconvolution techniques and substructuring approaches is given in section 2. A numerical benchmark for the comparison of deconvolution strategies is presented in section 3. An experimental 1D coupling scenario is shown in section 4, while a more practical multi-dimensional virtual point coupling is presented in section 5. Conclusive remarks are provided in section 6.

2 Theoretical Background

2.1 On deconvolution of signals: Least-square deconvolution

Given two sequences $\mathbf{t} = [t[0], t[1], \cdots, t[Q-1]]$ (length Q) and $\mathbf{l} = [l[0], l[1], \cdots, l[M-1]]$ (length M) the linear convolution $\mathbf{o} = \mathbf{t} * \mathbf{l}$ can be written in a matrix-vector product as:

$$\underbrace{\begin{bmatrix} o[1] \\ o[2] \\ \vdots \\ o[N-1] \\ o[N] \end{bmatrix}}_{\mathbf{o}} = \underbrace{\begin{bmatrix} l[0] & 0 & \dots & 0 \\ l[1] & l[0] & \ddots & \vdots \\ \vdots & l[1] & \ddots & 0 \\ l[M-1] & \vdots & \ddots & l[0] \\ 0 & l[M-1] & \vdots & l[1] \\ \vdots & \ddots & \ddots & \vdots \\ 0 & \dots & 0 & l[M-1] \end{bmatrix}}_{\mathbf{L}_c} \underbrace{\begin{bmatrix} t[0] \\ t[1] \\ \vdots \\ t[Q-1] \end{bmatrix}}_{\mathbf{t}} \tag{1}$$

where $\mathbf{L}_c$ is the so-called convolution (Toeplitz) matrix and the response $\mathbf{o}$ is of size $N = Q + M - 1$.
The Least-squares deconvolution to obtain $\mathbf{t}$ starting from $\mathbf{l}$ and $\mathbf{o}$ is defined by inverting the operation in eq. (1) via pseudo-inverse:

$$\mathbf{t} = \left(\mathbf{L}_c^T \mathbf{L}_c\right)^{-1} \mathbf{L}_c^T \mathbf{o} \tag{2}$$

If the output signal $\mathbf{o}$ is corrupted by error of random nature, the deconvolution process will lead to undesired error amplification due to the ill-conditioned nature of the convolution matrix. Regularization techniques such as Tikhonov $\mathbf{t} = \left(\mathbf{L}_c^T \mathbf{L}_c + \alpha \mathbf{I}\right)^{-1} \mathbf{L}_c^T \mathbf{o}$, where α is the regularization parameter, or truncated singular value decomposition $\mathbf{t} = \mathbf{V}_r \mathbf{S}_r^{-1} \mathbf{U}_r^H \mathbf{o}$, where $\mathbf{USV}$ represent the decomposition of $\mathbf{L}_c$ and r the set of retained SVs, may remedy this issue.
In the context of time sequences and impact testing, $\mathbf{o}, \mathbf{t}, \mathbf{l}$ represent impulse response, impulse response function and impulse load respectively. In case of multiple impacts, an averaging process can be integrated in eq. (2) leading to the IRF analog of the popular H_1 estimator for FRF.

2.2 On deconvolution of signals: Zero-padded circular deconvolution

Given the same two sequences $\mathbf{t}$ and $\mathbf{l}$ introduced in section 2.1, the circular convolution $\mathbf{o} = \mathbf{t} \circledast \mathbf{l}$ will perform the convolution as the inverse discrete/fast Fourier transform (iDFT/iFFT) of the product of the discrete/fast Fourier transform (DFT/FFT) of $\mathbf{t}$ and $\mathbf{l}$. The resulting signal differs from the linear convolution due to the periodic continuation enforced by the transformation in the frequency domain. Correct results are achieved when the signals are padded with zeros, such that their length is equal to the length of the resulting linear convolution, i.e. $N = Q + M - 1$.

In terms of deconvolution, assuming $M < N$, the process to estimate $\mathbf{t}$ is defined as follows:

1. Zero-pad the signal $\mathbf{l}$ to match the size of $\mathbf{o}$: $\tilde{\mathbf{l}} = [l[0], l[1], \dots, l[M-1], 0, \dots, 0]$ (length N)
2. Compute the FFTs of the signals: $\tilde{\mathbf{L}} = \text{FFT}(\tilde{\mathbf{l}}), \quad \mathbf{O} = \text{FFT}(\mathbf{o})$
3. Estimate $\mathbf{T}$ by division in the frequency domain: $\mathbf{T} = \dfrac{\mathbf{O}}{\tilde{\mathbf{L}}}$
4. Recover $\mathbf{t}$ by inverse FFT: $\mathbf{t} = \text{iFFT}(\mathbf{T})$

In case of output signal $\mathbf{o}$ corrupted by random error, a regularization can be achieved in the frequency domain using a Wiener filter in step 3 as $\mathbf{T} = \left(\dfrac{\tilde{\mathbf{L}}^*}{|\tilde{\mathbf{L}}|^2 + \frac{1}{S_n}} \right) \mathbf{O}$, where $()^*$ represents the conjugate, $||$ the

magnitude and S_n the signal-to-noise ratio.
Note that, similarly to what was described at the end of section 2.1, in the context of time sequences and impact testing, step 3 can be replaced by a H_1 averaged FRF estimation.

2.3 Frequency Based Substructuring

The assembly of substructures in the frequency domain is performed according to the Lagrange Multiplier-Frequency Based Substructuring (LM-FBS) formulation [2]. In the following, all operations are performed per frequency line. The compatibility of displacement and equilibrium of forces are imposed to the collocated DoFs of the substructures' admittances to be coupled:

$$\begin{cases} \mathbf{u}(f) = \mathbf{Y}(f)(\mathbf{f}(f) - \mathbf{B}^T\boldsymbol{\lambda}(f)) \\ \mathbf{B}\mathbf{u}(f) = \mathbf{0} \end{cases}, \mathbf{Y} = \begin{bmatrix} \mathbf{Y}^{(1)}(f) & \mathbf{0} & \cdots & \mathbf{0} \\ \mathbf{0} & \mathbf{Y}^{(s)}(f) & \ddots & \vdots \\ \vdots & \ddots & \ddots & \mathbf{0} \\ \mathbf{0} & \cdots & \mathbf{0} & \mathbf{Y}^{(N_s)}(f) \end{bmatrix} \tag{3}$$

where $\mathbf{u}(f)$ and $\mathbf{f}(f)$ are the concatenated vectors of displacements and applied forces of each substructure (s), (N_s) is the total number of substructures, $\boldsymbol{\lambda}(f)$ is a set of Lagrange multipliers describing the interface force intensities, $\mathbf{Y}(f)$ is a matrix of frequency response functions (FRFs), $\mathbf{B}$ is the signed Boolean matrix matching the corresponding DoFs.
The equations are solved in closed form by evaluating the $\boldsymbol{\lambda}(f)$ that close the interface gap $\mathbf{g}(f) = \mathbf{B}\mathbf{Y}(f)\mathbf{f}(f)$:

$$\left(\mathbf{B}\mathbf{Y}(f)\mathbf{B}^T\right)\boldsymbol{\lambda}(f) = \mathbf{g}(f) \tag{4}$$

Finally, the assembled response is computed as:

$$\mathbf{u}^{AB}(f) = \underbrace{\left[\mathbf{I} - \mathbf{Y}(f)\mathbf{B}^T\left(\mathbf{B}\mathbf{Y}(f)\mathbf{B}^T\right)^{-1}\mathbf{B}\right]\mathbf{Y}(f)}_{\mathbf{Y}^{AB}(f)}\mathbf{f}(f) \tag{5}$$

2.4 Impulse Based Substructuring

The time-analog to LM-FBS, i.e. Impulse Based Substructuring (IBS), is performed by means of a convolution scheme [5]:

$$\begin{cases} \mathbf{u}^{(s)}(t) = \int_0^t \mathbf{H}^{(s)}(t-\tau)\left(\mathbf{f}^{(s)}(\tau) + \mathbf{B}^{(s)^T}\boldsymbol{\lambda}(\tau)\right)d\tau \\ \sum_{s=1}^{N_S}\mathbf{B}^{(s)}\mathbf{u}^{(s)}(t) = \mathbf{0} \end{cases} \tag{6}$$

where the same notation as in section 2.3 is used, but with time-based quantities, and $\mathbf{H}(t)$ is a matrix of impulse response functions (IRFs).
The convolution integral is solved incrementally following a discretization procedure [5, 6]. At each discrete time step k, the assembled response is evaluated by $\mathbf{u}^{AB}[k] = \tilde{\mathbf{u}}^{(s)}[k] + \mathbf{u}_\lambda^{(s)}[k]$, where $\tilde{\mathbf{u}}^{(s)}[k]$ is the predicted response that misses the Lagrange multipliers $\boldsymbol{\lambda}[k-1]$ and $\mathbf{u}_\lambda^{(s)}[k]$ is the correction that closes the current time step gap $\mathbf{g}[k] = \sum_{s=1}^{N_S}\mathbf{B}^{(s)}\tilde{\mathbf{u}}^{(s)}[k]$. The Lagrange multipliers used to close that gap are computed as:

$$\left(\sum_{s=1}^{N_S}\mathbf{B}^{(s)}\mathbf{H}^{(s)}[0]\mathbf{B}^{(s)^T}\right)\boldsymbol{\lambda}[k-1] = -\sum_{s=1}^{N_S}\mathbf{B}^{(s)}\tilde{\mathbf{u}}^{(s)}[k]\cdot\frac{1}{\Delta t} \tag{7}$$

2.5 Shock Response Prediction

To estimate the temporal response signal of a sudden event using substructuring, the transfer function from the input to the output location should be measured and then the external force applied. To achieve this, both a time-based and a frequency-based approach may be adopted:

- Impulse Based Substructuring with Least-square deconvolution. This approach relies on IRFs computed via the Least-square method introduced in section 2.1 [1] and a recursive estimation of the assembled response prediction via the IBS algorithm of section 2.4.
- Frequency Based Substructuring with zero-padded circular deconvolution. This approach relies on FRFs for the construction of the assembled system as in section 2.3, followed by a frequency-based deconvolution as in section 2.2. The latter enables the re-construction of the target time-based response from the FBS prediction and can be evaluated by iFFT($\mathbf{u}^{AB}(f)$) (solution (1)) or, alternatively, iFFT($\mathbf{Y}^{AB}(f)$) $*$ $\mathbf{f}(t)$ (solution (2)).

3 Impulse Response Function Estimation via Deconvolution: A Numerical Case

The deconvolution techniques presented in section 2.1 and section 2.2 are investigated on a simple numerical benchmark. All calculations are performed in Matlab. An impulse force l is approximated as $l = 2\exp\left(-0.8\left(n-5\right)^2\right)$ and an impulse response function t as $t = 10\left(0.95^n\right)\sin(0.2\pi n)$ with the time sequence n = linspace$(1, 300, 600)$. The signals l and t are then cut to size $M = 18$ and $Q = 300$. The corresponding impulse response is computed via linear convolution. The signals are visualized in fig. 1. Then, a random-distributed noise with magnitude 0.001 is added on the output o. The original and noisy output are given in fig. 2. The noise is rather small compared to the signal level. Finally, the impulse response function t is estimated for both original and noisy outputs with the deconvolution strategies (without and with regularization) highlighted in section 2.1 and section 2.2. From fig. 3-left (FFT(IRF) t) and fig. 4 (IRF t) it is evident that the time-based (Least-square) and frequency-based (zero-padded circular) deconvolution produce equivalent outcomes for the impulse response function. The effect of noise on the output is visualized in fig. 3-right (FFT(IRF) T) and fig. 5 (IRF t). The following considerations apply:

- Time (Least-square) and frequency (zero-padded circular) deconvolution both generate an erroneous estimation of the impulse response function t. Both estimated signals coincide in the central portion but exhibit differences at the extremes due to varying responses to noise by the algorithms. Time-based deconvolution maintains accuracy in the initial and final time steps of t and propagates the error away from the time-boundaries. Conversely, frequency-based deconvolution spreads errors at both ends. The discrepancy in the number of sequence steps correlates with the length of the force signal l.
- Regularization strategies work differently in the time and frequency domains, but have great potential to limit the influence of noise in the transfer estimation (at least when the output error is of purely random nature). The parameters of the regularization functions have been manually tuned ($\alpha = 0.1$ for Tikhonov, threshold$= 0.5$ for SVD truncation, $S_n = 1000$ for Wiener).

The effect of other processing parameters/operations has been investigated, such as the influence of additional (left and right) zero-padding for both force l and output o sequences and windowing. None of this is presented here, as no significant findings have been observed for the present case.

4 Experimental 1D Substructuring Example

For the 1D experimental test case, two aluminum rods are assembled via a single-DoF compatibility condition and the result compared with a reference monolithic rod. All calculations are performed in Python.

[1] The use of frequency-based techniques such as zero-padded circular deconvolution for IRFs estimation would also be possible, but would contradict the goal of bypassing the Fourier transform.

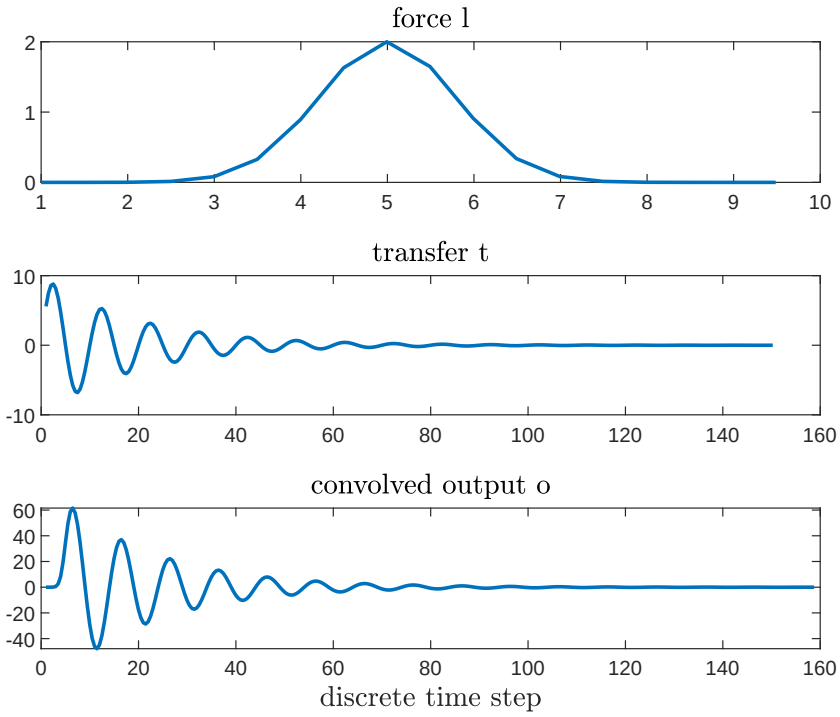

Figure 1: Impulse force l, impulse response function t and corresponding convolved impulse response o.

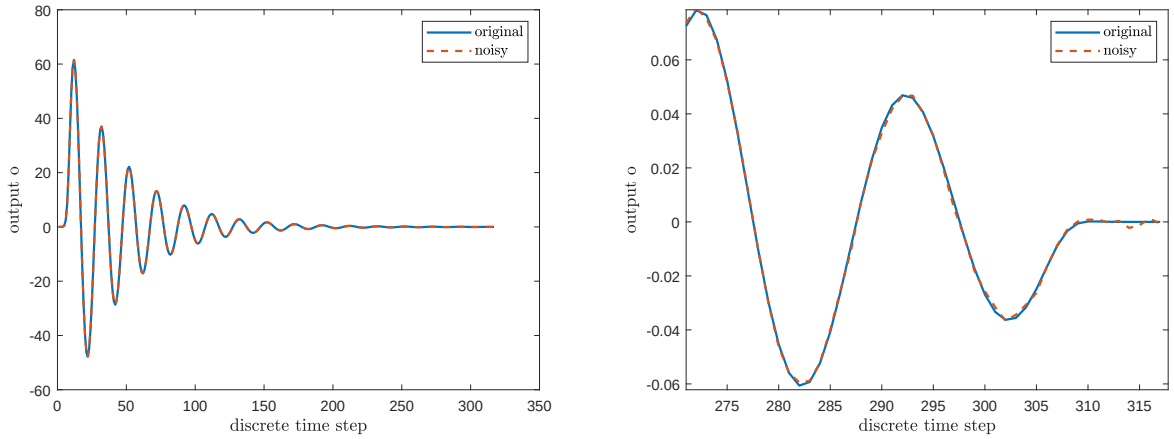

Figure 2: Reference and noise-polluted impulse response o. Left: full signal. Right: zoom at end of signal.

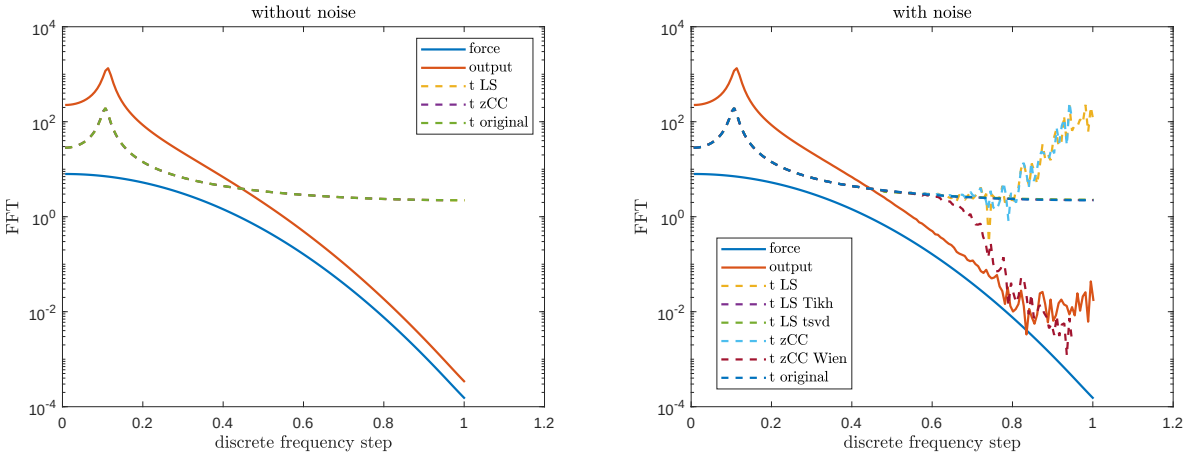

Figure 3: Fast-Fourier Transform (FFT) of impulse response function t estimated with Least-square (LS), Least-square w. Tikhonov (LS Tikh), Least-square w. TSVD (LS tsvd), zero-padded circular deconvolution (zCC), zero-padded circular deconvolution w. Wiener filter (zCC Wien). Comparison with reference/original. Left: without noise. Right: with noise.

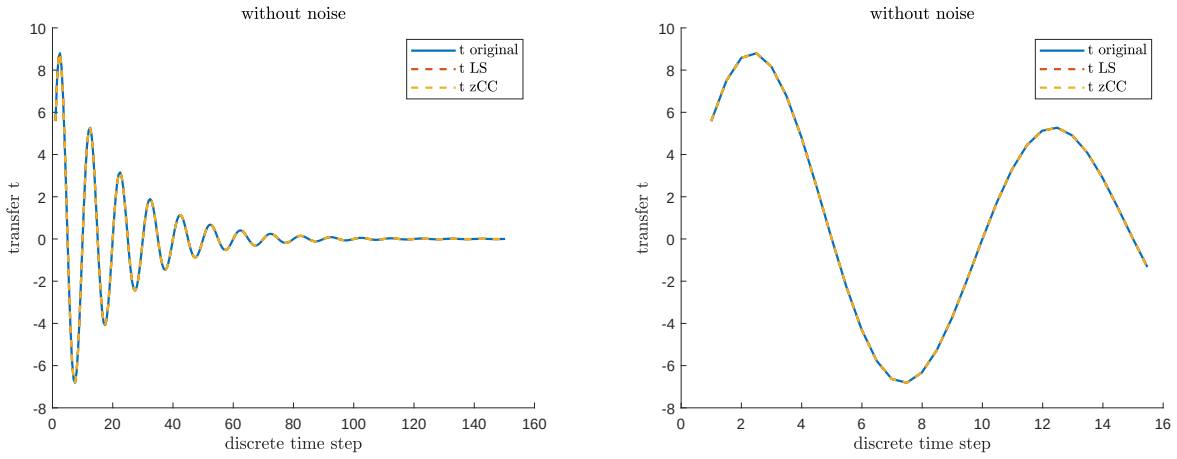

Figure 4: Impulse response function t using the reference output estimated with Least-square (LS), zero-padded circular deconvolution (zCC). Comparison with reference/original. Left: full signal. Right: zoom at beginning of signal.

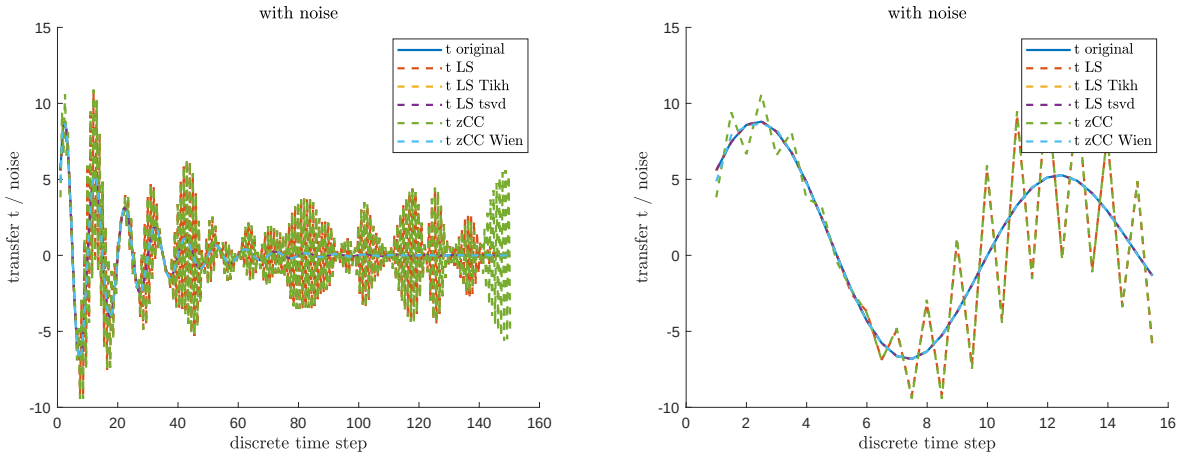

Figure 5: Impulse response function t using the noisy output estimated with Least-square (LS), Least-square w. Tikhonov (LS Tikh), Least-square w. TSVD (LS tsvd), zero-padded circular deconvolution (zCC), zero-padded circular deconvolution w. Wiener filter (zCC Wien). Comparison with reference/original. Left: full signal. Right: zoom at beginning of signal.

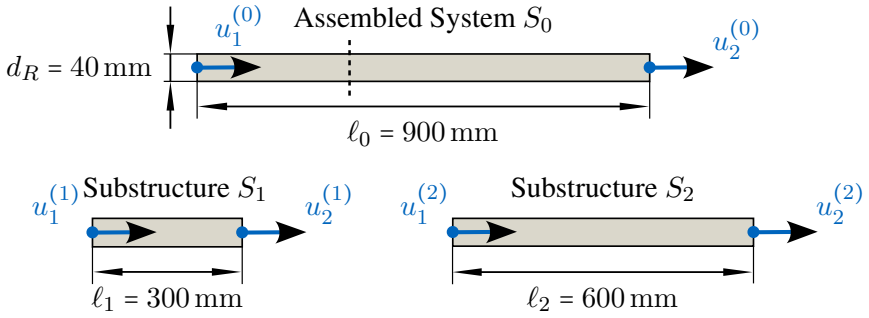

Figure 6: Overview of geometry and coordinates of the one-dimensional rods considered as test pieces [7].

Description of the rods' dimensions and corresponding DoFs are provided in fig. 6. A steel tip hammer and piezo-accelerometers are used to acquire the necessary raw time signals on the free-floating components with a sampling rate of 102.4 kHz. Further details about the measurement setup are given in [6]. The data processing is performed according to FBS (section 2.3) and IBS (section 2.4) and the corresponding predictions are compared. No regularization is performed.

In fig. 7, the FBS coupling prediction is evaluated against the assembled reference in the frequency domain. The result shows that an axial 1D coupling is a good, albeit incomplete, fit to describe the dynamics of the aluminum bar. In particular, the coupled damping seems to be quite lower than the expected reference.
The result of the shock response prediction according to section 2.5 is provided in fig. 8 for the driving-point transfer in u_1^0 using one of the measured forces on the assembled system in u_1^0. The following considerations apply:

- The two FBS alternatives to retrieve the time output signal are identical but at the beginning of the sequence, where the effect of the forced periodization is present, thus the FBS result is erroneous. FBS otherwise provides stable results over the entire time span analyzed.
- The IBS prediction becomes quickly unstable due to error propagation issues [6] but it represents the correct solution right at the beginning of the sequence.
- Although different assembly computations and potentially different available data processing, the FBS and IBS predictions should ideally deliver the same result away from the signal boundaries (indicated by the black vertical line, i.e. the length of the non-padded impulse). However, there are discrepancies

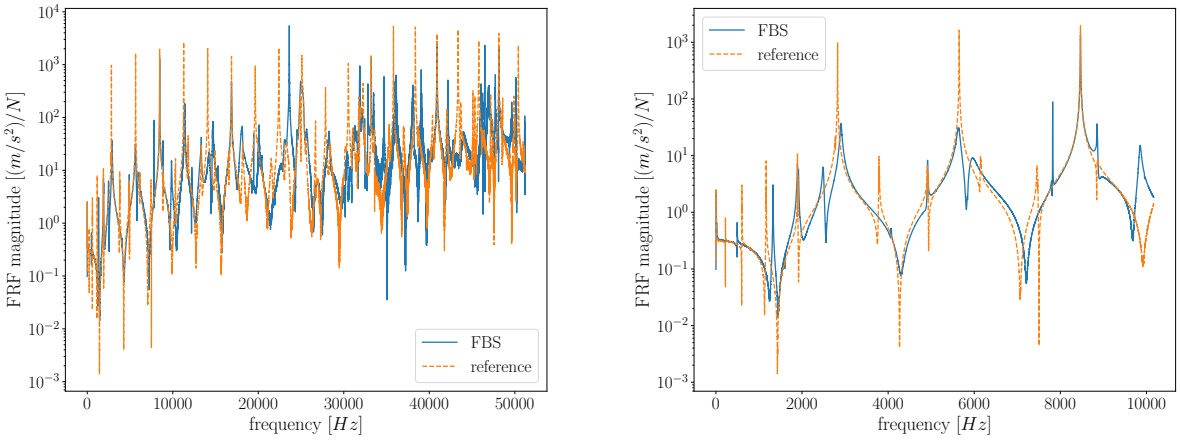

Figure 7: Comparison between FBS prediction and reference measurement for the input and output in u_1^0. Left: full available frequency domain. Right: zoom on first 10000 Hz.

between the time and frequency predictions that require further investigation [2].

5 Experimental 3D Substructuring Example

The experimental 3D benchmark consists of the AM benchmark, i.e. two aluminum components connected with a screw joint and washers. The coupling of the two substructures is compared with some reference measurements on the assembled system. All calculations are performed in Python using the open-source package pyFBS [8]. The benchmark together with the design of experiments is shown in fig. 9. A vinyl tip hammer and piezo-accelerometers are used to acquire the raw time signals with a sampling rate of $102.4\,\mathrm{kHz}$ on the free-floating components. Further details about the measurement campaign can be found in [7]. The Virtual Point Transformation is used for the interface description to ensure the coupling of 3 translational and 3 rotational DoFs [9]. The substructuring coupling methods for FBS (section 2.3) and IBS (section 2.4) are then used to obtain predictions for the assembled system. In the IBS case, a downsampling (with low-pass filtering) with factor $x7$ is applied to the data in order to limit the error propagation during convolution (see [7, 6]). The data for the FBS processing are left unaltered. No regularization is performed.

Analog to the 1D case, the result of the FBS prediction is first evaluated against the frequency-based assembled reference in fig. 10. The 6 DoFs virtual point coupling leads to a successful prediction, especially in the low-medium frequency regime ($< 5\,\mathrm{kHz}$) where the signal-to-noise ratio is significantly high.
The resulting prediction of the shock response according to section 2.5 is then shown in fig. 11 for the transfer associated with the output in $S10_z$ and the input in H_1 using one of the impulses applied to the assembled system in H_1. Analogous considerations apply as described for section 4. Here, for the sake of simplicity, only the solution (1) for the FBS reconstruction is considered. The periodization error in the frequency convolution is once again apparent. Similar considerations apply to the accuracy of IBS at the beginning of the time sequence and to the overall stability and discordance between IBS and FBS predictions.

6 Conclusion

A comparative analysis is performed between frequency- and impulse-based substructuring in the context of experimental shock response predictions. Focus is given on the deconvolution algorithms used in time

[2] One of the causes of the discrepancies is clearly the amplification/propagation of the error during the convolution process of the IBS.

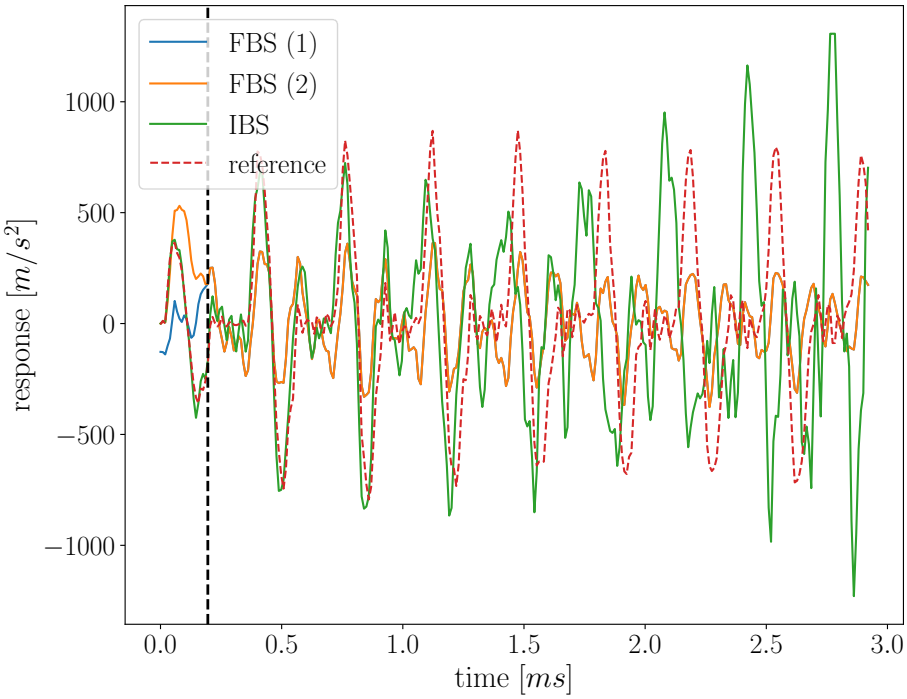

Figure 8: Shock response prediction (first 3 ms) for the 1D case. Comparison between FBS (solution (1), see section 2.5), FBS (solution (2), see section 2.5), IBS and reference measurement for the output and input in u_1^0. The input force is the assembled system impulse in u_1^0. The black vertical line indicates the max. steps of the non-padded force signal.

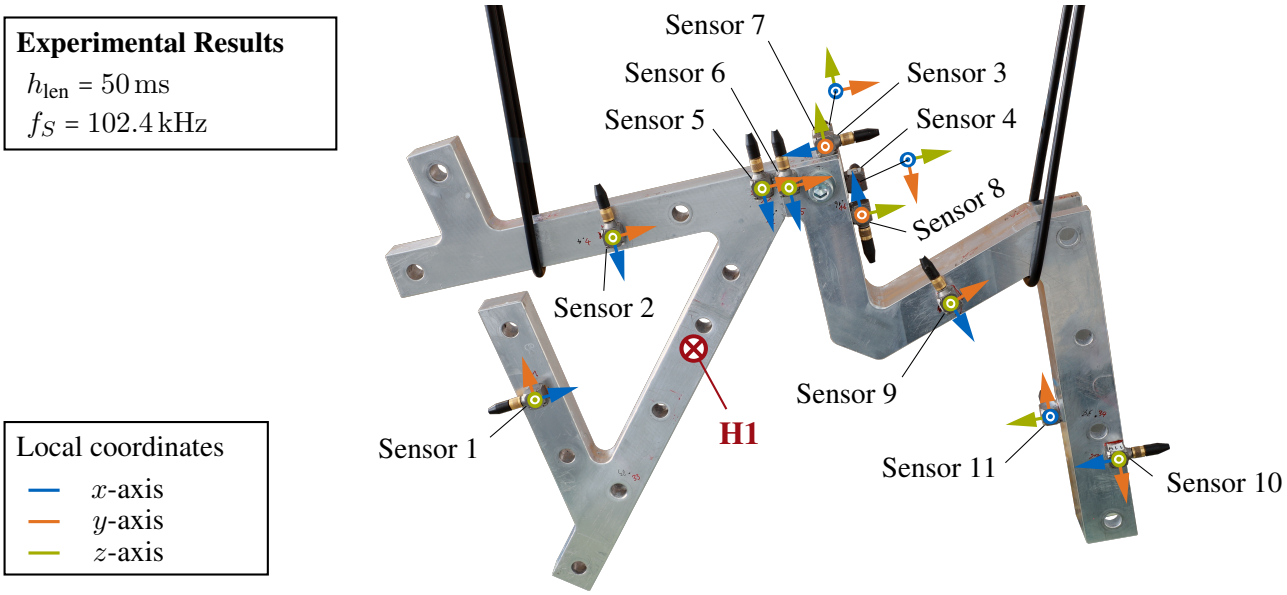

Figure 9: Overview of design of experiments on the assembled system of the AM benchmark in pyFBS. Highlighted in text are the processing parameters for IBS, i.e. the length of the IRF processed h_{len} and the acquisition sampling rate f_S [7].

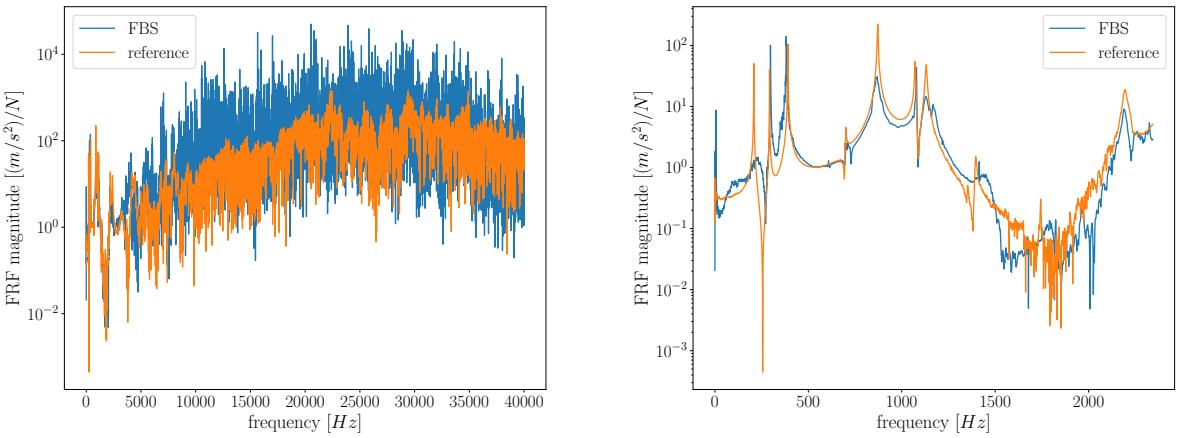

Figure 10: Comparison between FBS prediction and reference measurement for the output in $S10_z$ and the input in H_1. Left: full available frequency domain. Right: zoom on first 2300 Hz.

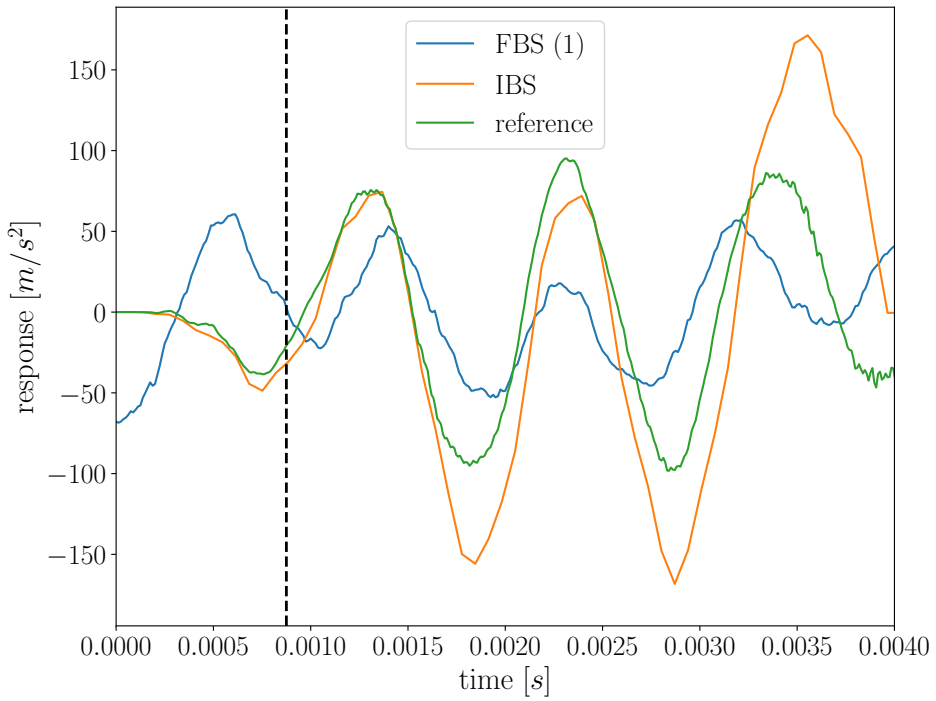

Figure 11: Shock response prediction (first 4 ms) for the 3D case. Comparison between FBS (solution (1), see section 2.5), IBS and reference measurement for the output in $S10_z$ and the input in H_1. The input force is the assembled system impulse in H_1. The black vertical line indicates the max. steps of the non-padded force signal.

(Least-square) and frequency (zero-padded circular deconvolution) domain.
A numerical study of the deconvolution process to estimate impulse response functions reveal that the equivalence between the time and frequency deconvolution is lost as soon as an error (here in the form of random noise) is introduced into the output signal. Regularization techniques seem to be promising for such a simple scenario. Both a 1D and a multi-dimensional (virtual point) experimental substructuring coupling case are analyzed. Unsurprisingly, the same periodization error of the frequency deconvolution appears in the shock prediction of FBS, which solution is otherwise stable in time. Viceversa, IBS provides accurate results at the beginning of the signal before it quickly becomes unstable.
Further investigations are required to assess the discrepancies between FBS and IBS shock predictions outside the 'boundary' time-frame. Finally, corrections are sought for the behaviour of FBS and IBS in the respective erroneous regimes.

References

[1] Bjorn Jetmundsen, Richard L. Bielawa, and William G. Flannelly. "Generalized Frequency Domain Substructure Synthesis." In: *Journal of the American Helicopter Society* 33.1 (1988), pp. 55–64. ISSN: 00028711. DOI: 10.4050/jahs.33.1.55.

[2] D. De Klerk, D. J. Rixen, and J. De Jong. "The frequency based substructuring (FBS) method reformulated according to the dual domain decomposition method". In: *24th International Modal Analysis Conference*. "St.Louis, MO", 2006.

[3] J. Gordis and J. Radwick. "Efficient transient analysis for large locally nonlinear structures". In: *Shock and Vibration* 6.1 (1999), pp. 1–9.

[4] J. Gordis. "Fast Transient Analysis for Locally Nonlinear Structures by Recursive Block Convolution". In: *Journal of Vibration and Acoustics* 123 (2001), pp. 545–547.

[5] D. J. Rixen. "Substructuring using Impulse Response Functions for Impact Analysis". In: *Proceedings of the IMAC-XXVIII* (2011). DOI: 10.1007/978-1-4419-9834-7_56.

[6] O. M. Zobel, F. Trainotti, and D. J. Rixen. *Enabling Experimental Impulse-Based Substructuring through Time Domain Deconvolution and Downsampling*. 2024. arXiv: 2404.14802 [physics.app-ph].

[7] O. Zobel. "Experimental Impulse Based Substructuring: A Time-Domain Solution for Modular Structural Dynamics". Master's thesis. Garching: TUM School of Engineering and Design, Nov. 2023.

[8] Tomaž Bregar et al. "pyFBS: A Python package for Frequency Based Substructuring". In: *Journal of Open Source Software* 7.69 (2022), p. 3399. DOI: 10.21105/joss.03399.

[9] Maarten Vicent Van der Seijs. "Experimental Dynamic Substructures: Analysis and Design Strategies for Vehicle Developement". In: *Doctoral Thesis* (2016), p. 208.